Quench Propagation in Nb_3Sn cos-theta 11 T Dipole Model Magnets in High Stress Areas

F.J. Mangiarotti, G.P. Willering, H. Bajas, M. Bajko, B. Bordini, L. Bottura, S. Izquierdo Bermudez, C.H. Löffler, J.V. Lorenzo Gomez, F. Savary, M. Probst

***Abstract*—A large number of training quenches at various currents, temperatures and ramp rates, have been performed on six 11 T dipole model magnets. Quenches in the midplane of these magnets were of special interest, since the quench current in the last three models measured in 2016 was limited to between 84 and 92% of the magnets short sample limit. Measurements of quench propagation velocity, based on both voltage taps and quench antennas, yield a high propagation velocity of 50 to 80 m/s. Due to the high magnetic field gradient over the width of the midplane turn such a high propagation speed cannot be explained by propagation in longitudinal direction of the strand following the twist pitch. In these cases, current and heat sharing at the thin cable edge (where the field, stress and cable compaction are high) are likely to provoke strand-to-strand quench propagation at higher velocities than along the strands. This investigation is focused on analyzing the quench propagation along the strands and strand-to-strand of various measured cases.**

***Index Terms*—Nb_3Sn , Quench Propagation Velocity, Superconducting Magnets.**

I. Introduction

In the framework of the High Luminosity LHC project (HL-LHC) at CERN it is planned to replace some of the 1232 NbTi 8.3 T LHC main dipoles (MB) with Nb_3Sn magnets (MBH) with a magnetic field of 11 T [1]. The powering performance of six 2-m-long models of these magnets has been published in [2], [3], [4]. Nine cos-theta coils have been tested in single aperture (with two coils) and double aperture (with four coils) configurations; some coils have been tested in more than one magnet assembly. A summary of the tests is presented in Table I.

A magnetic field and stress profile of the magnets at or above nominal current are shown in Fig 1. The inner pole turn is the area with the highest magnetic field, and the magnetic field gradient is relatively low (9.7 to 11.8 T at nominal current across the width of the cable); in that region the stresses are the lowest. The inner midplane turn is where the stresses are largest, the peak magnetic field is slightly lower than in the inner pole turn but the gradients are much larger (3.7 to 11.3 T at nominal current). The stress in these two regions are studied in [5]; depending on the magnet, the stress in the inner pole turn at nominal current is around 30–83 MPa, and in the inner midplane 120–155 MPa.

A recent test of the pressure distribution in the inner midplane of magnet SP_105 after pre-loading at room temperature (Fig 2) with Fujifilm Prescale pressure measurement film shows a large stress gradient across the cable, much larger than the predicted by the numerical simulations in these conditions. The stress gradient is caused by the C-shape mica insulation in the cables,a design implemented for its advantages during manufacturing but that does not cover the entire width of the cables. This gradient is probably also present during the high current powering of the magnets.

During the test of the last dipole (SP_105) a high quench

F.J. Mangiarotti, G.P. Willering, H. Bajas, M. Bajko, B. Bordini, L. Bottura, S. Izquierdo Bermudez, C.H. Löffler, J.V. Lorenzo Gomez, F. Savary, M. Probst are with CERN, CH-1211, Geneva, Switzerland (email: franco.julio.mangiarotti@cern.ch).

Manuscript received XXXX.

TABLE I
Summary of the powering tests in the 11 T dipole model magnets.

Magnet	Coils	Test date	Max. Current
SP_101	106, 107	Oct 2014	11921 A
SP_102	106, 108	May 2015	12794 A
SP_103	109, 111	Sep 2015	12246 A
DP_101	106, 108, 109, 111	Dec 2015	13205 A
SP_104	112, 113	Jun 2016	11734 A
SP_105	114, 115	Nov 2016	12379 A

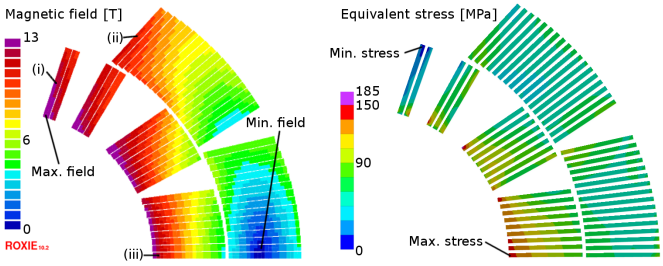

Fig. 1. Profiles of one quadrant of a double aperture magnet, at the nominal current of 13200 A: magnetic field (right) and stress (left). Three turns are labeled: inner pole turn (i), outer pole turn (ii), inner midplane (iii). The highest stress areas are near the inner midplane, a location where the maximum magnetic field is close to maximum. Color version available online.

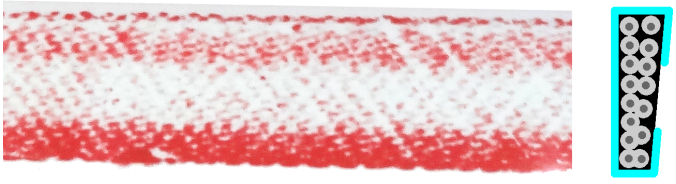

Fig. 2. Left: pressure distribution in the inner midplane turns of SP_105, after preloading at room temperature. Right: schematic cross section of the cable of the 11 T dipole model magnets, showing the C-shape mica insulation (blue). In both figures the magnet bore is at the bottom. As the mica insulation does not cover the cable completely, it provokes a non-uniform stress distribution across the cable.

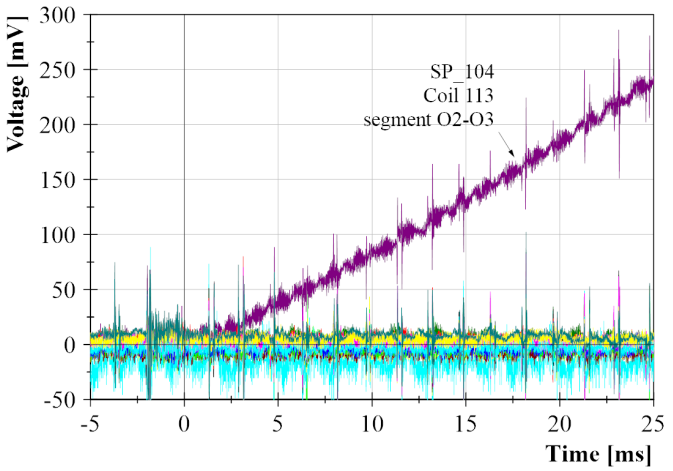

Fig. 3. Example of single-segment voltage rise after a quench. The quench starts at time = 0. Only quenches with voltage rise in a single segment or two consecutive segments are analyzed in this paper.

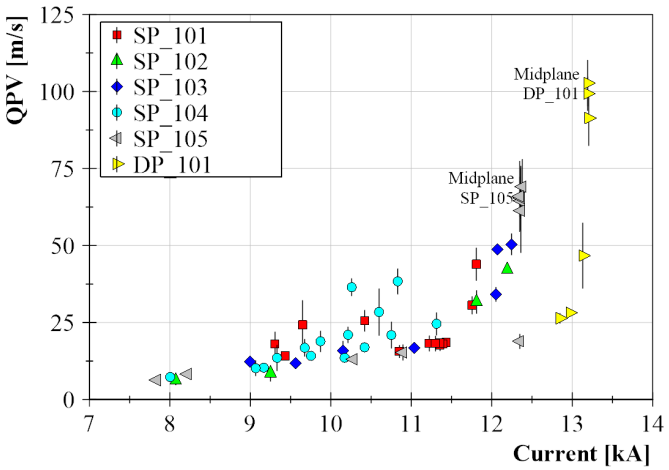

Fig. 4. Measured QPV of the qualified quenches in all tested 11 T dipole magnets.

propagation velocity (QPV) was observed for quenches originating in the magnet's midplane, the area where the stress is larger and the magnetic field gradient is maximum. Quench propagation on Nb_3Sn Rutherford cables has been studied and modeled before [6], [7], [8], but for configurations without a magnetic field gradient across the width of the cable. This motivated an investigation on the quench propagation of quenches in all the 11 T model magnets. In this paper we analyze the quench data of the six magnets and compare them with numerical simulations.

II. Quenches in the 11 T Nb_3Sn model dipoles

The magnets were instrumented with a series of voltage taps along their winding. In case of quench during powering, the voltage difference between consecutive pairs of voltage taps was measured. In most cases, the evolution of the voltage signals after quench follows one of these three patterns: (a) the voltage rises only in one or two consecutive voltage taps segments (see Fig 3), (b) the voltage rises in two adjacent but not consecutive segments, or (c) the voltage rises in two or more non-adjacent segments.

Patterns (b) and (c) indicate that a non-local effect caused the quench, and as such energy deposition over a relative long cable length and/or multiple turns is expected. In these cases the number of quench fronts is difficult to reliably determine; in addition, the distributed energy deposition will increase the temperature of the superconductor and thus affect the QPV. Quenches with these patterns were thus excluded from the analysis. In addition, quenches provoked by known defects (such as quenches in the layer jump in SP_104, coil 113, as discussed in [4]) are discarded. These criteria leave us with 45 quench instances to analyze out of the 144 total quenches between the six magnets.

The QPV was estimated from the rate of voltage rise after quench as follows:

$$QPV = \frac{1}{n_f}\frac{dl_R}{dt} \approx \frac{A_{cu}}{n_f I \rho_{cu}}\frac{dV_R}{dt} \qquad (1)$$

where n_f is the number of quench propagation fronts, l_R the length of the cable that became resistive, A_{cu} the cross-sectional area of copper in the cable, I the current in the magnet, ρ_{cu} the resistivity of copper at the quench location and V_R the resistive voltage. This equation assumes that the resistivity of copper is constant and uniform in the entire quenched segment, and thus is accurate only before the temperature rises significantly.

The QPV was estimated in two regions: in a few millisecond range close to the quench start, after transients had finished, and in the range where the resistive voltage was between 50 and 150 mV using equation (1). In these ranges the hotspot temperature typically does not exceed 30–40 K, which corresponds to an overestimation of the QPV by 3–14 %. In addition, in some quenches we used a quench antenna to localize the quench, and we could estimate the QPV from the delay of the onset of the signals on different coils. The average QPV was estimated from these values, and the standard deviation of the values is used as an estimation of the uncertainty.

The data of QPV as a function of quench current for the six model magnets is presented in Fig. 4. For a given current, the QPV has a minimum which is given by the "ideal" quench situation: the energy of the disturbance that caused the quench is minimum, and the critical current of the cable has not been reduced by any reason. Higher velocities may be caused by either a large disturbance or a reduced critical current. A large, distributed energy disturbance (i.e. a slip-stick motion of a cable in the winding) can explain single large QPV events; however a reduced critical current is the more probable cause of repetitive, high QPV quenches. In particular, the midplane quenches in magnets SP_105 and DP_101 that have a very large quench propagation velocity seem to be caused by a reduction of critical current, as they are at the same current level and in the same range of QPV.

III. 1-D lumped model simulation results

The model utilized to perform the quench propagation simulations was developed in MATLAB specifically for Nb_3Sn

magnets, as described in [9]. This lumped model assumes uniform temperature in each component at every section of the cable, and thus the temperature distribution along the cable is modeled in one dimension. The heat exchange between different components is modelled by means of thermal resistances. At each section, the superconductor carries all the current up to the local temperature-dependent critical current, with the copper carrying the rest of the current and generating Joule heating. The critical current dependency on magnetic field, temperature and strain is modeled according to the ITER-2008 parametrization [10]. The simulated geometry is a rectangular cable composed of Nb_3Sn, copper, and insulation, with the same average dimensions as the cables in the 11 T dipole models.

The simulations were performed at different current levels, using the cable properties (copper-superconductor ratio, RRR, Nb_3Sn critical surface parameters) of the nine coils. Three levels of the strain dependency function ($s(\epsilon)$ in the ITER-2008 parametrization) were considered: 1 (i.e. no strain), 0.9 (approximately equivalent to an uniaxial strain of 0.4 %) and 0.8 (approximately equivalent to an uniaxial strain of 0.6 %).

Two quench propagation mechanisms have been considered: by heat conduction Along The quenched Strand (ATS) or from Strand To Strand (STS) by either heat conduction or joule heating produced by current redistribution. The QPV for the STS mechanism in the Rutherford cable is estimated as the QPV for a parallel strand cable in an uniform magnetic field — that is, the current redistribution during quench is not simulated with this model. Since the Nb_3Sn strands are heat-treated after magnet winding, the strand-to-strand contact is expected to be relatively good, especially at the cable edge with high compaction factor, and therefore this estimation of the STS QPV should be a good approximation. The QPV is calculated from (1) as:

$$QPV_{STS} = \frac{1}{2}\frac{dL_{cs}}{dt} \tag{2}$$

where L_{cs} is the length of the cable at a temperature higher than the current sharing temperature, and the factor $1/2$ takes into account the two propagation fronts. The magnetic field applied to the cable was assumed to be directly proportional to the transport current. The magnetic field at nominal current (11850 A) was set to be the maximum nominal magnetic field in the corresponding cable location: 11.8 T for the inner pole turn, 11.3 T for the inner midplane, and 10.3 T for the outer pole turn simulations.

Since the magnetic field is modeled as uniform across the cable, to be able to estimate the QPV for the ATS mechanism, we performed a series of simulations at different magnetic fields, between the minimum and the maximum nominal field in the corresponding cable location: 9.6–11.8 T in the inner pole turn, 3.7–11.3 T in the inner midplane, and 7.8–10.3 T in the outer pole turn. As the magnetic field distribution across the cable is approximately linear, the average QPV is calculated as:

$$QPV_{ATS} = \cos(\alpha)\left(\int_{B_{min}}^{B_{max}} \frac{1}{QPV(B)}\frac{dB}{B_{max}-B_{min}}\right)^{-1} \tag{3}$$

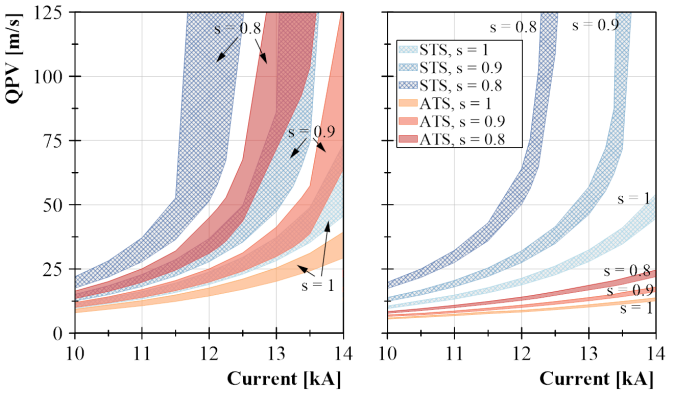

Fig. 5. QPV as function of transport current obtained from simulation of quenches in the inner pole turn (left) and inner midplane (right), with strain function s from 0.8 to 1, for both STS (in blue with cross pattern) and ATS (in red) propagation mechanisms.

where α is the twist pitch angle, B is the magnetic field across the width of the cable, and B_{max} and B_{min} are the maximum and minimum magnetic field in the cable cross section, respectively.

A model to estimate the QPV for a third quench propagation mechanism composed of a combination of ATS and STS propagation is currently under development. The QPV in this case is expected to be larger than the ATS QPV and lower than the STS QPV, since the current redistribution during quench is not simulated in the STS case.

The results of QPV as function of transport current are shown in Fig 5 for the inner pole turn and the inner midplane simulations. The bands represent the results at the same current and strain level of simulations using the cable parameters from the different coils. The bands are thinner for the midplane simulations due to fewer cable parameters being simulated – only those from the coils that had analyzed midplane quenches. The STS and ATS results are relatively similar for the inner pole turn case; however in the inner midplane the STS and ATS are very different, due to the high magnetic field gradient in the latter cable location. In both cases a decrease in the strain function (corresponding to higher strain levels in the cable) provoke an increase of the QPV.

IV. Discussion

The experimental and the simulation results are compared in Figs 6, 7 and 8 for the inner pole turn, outer pole turn and inner midplane data, respectively.

At the inner and outer pole turns, the measured QPV fits relatively well within the simulated values for both propagation mechanisms. However the ATS mechanism requires a higher strain to reach the same level of QPV of the STS mechanism. As the stress in the pole turn is very small, the STS mechanism is more likely to be the propagation mechanism of these quenches.

In the midplane quenches the difference between STS and ATS is much larger. The experimental data points fit much better to the STS bands, suggesting that the dominating propagation mechanism in this area is strand-to-strand. The

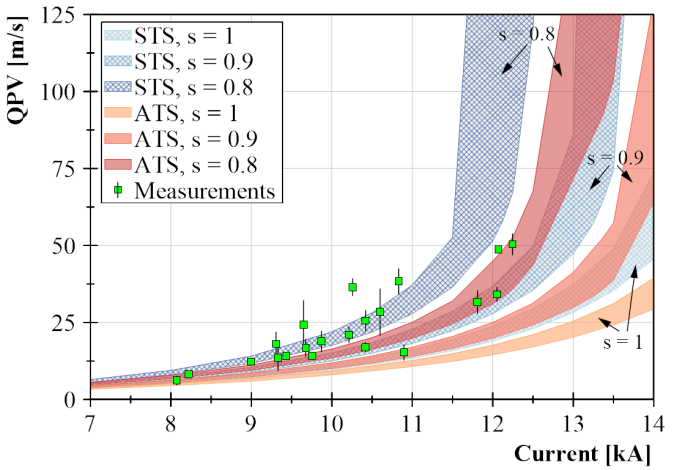

Fig. 6. QPV versus quench current plot of the measurements (in green squares) and the simulations for the STS (in blue with cross pattern) and ATS (in red) propagation mechanisms, at the inner pole turn.

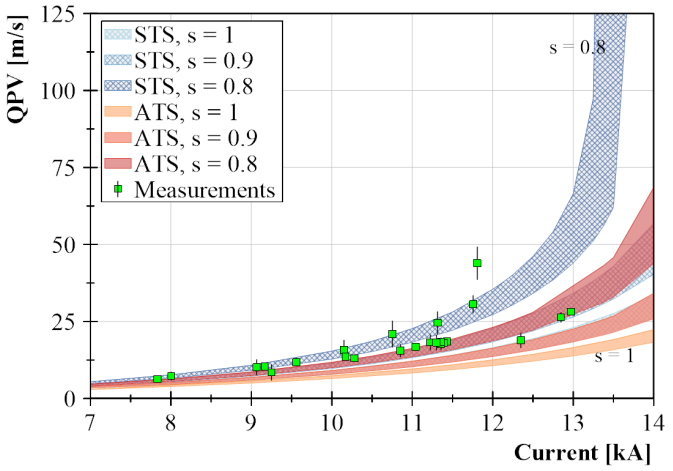

Fig. 7. QPV versus quench current plot of the measurements (in green squares) and the simulations for the STS (in blue with cross pattern) and ATS (in red) propagation mechanisms, at the outer pole turn. Note that there are two sets of overlapping bands: the "ATS, s=0.9" and "STS, s=1" bands (lower overlapping bands), and the "ATS, s=0.8" and "STS, s=0.9" bands (upper overlapping bands).

midplane quenches have much larger QPV than the expected from the calculation with zero strain ($s(\epsilon) = 1$). As the voltage rises linearly during those quenches, a local defect as a cause of the fast QPV is unlikely. A strain function $s(\epsilon)$ less than one is expected, because the midplane strands are subject to a high stress [5].

For magnet SP_105, the QPV of the six quenches in the midplane indicate a strain function around 0.8–0.9, which in turn corresponds to a critical current reduction at the quench magnetic field (around 12 T) of 25–50 %. The midplane quenches in magnet DP_101 are above the 0.9 strain function band, suggesting a critical current reduction at the quench magnetic field (around 13 T) of more than 30 %.

From [5], the expected transverse stress levels in the midplane in magnet SP_105 are about 134 MPa at nominal current, and in DP_101 about 144 MPa at the maximum test current (13.2 kA). From [11], in this situation, the expected critical

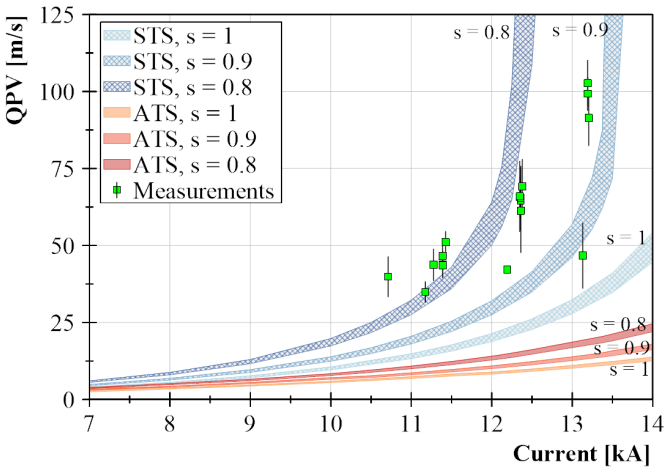

Fig. 8. QPV versus quench current plot of the measurements (in green squares) and the simulations for the STS (in blue with cross pattern) and ATS (in red) propagation mechanisms, at the inner midplane.

current reduction of the Nb_3Sn cables in the midplane of magnet SP_105 is around 12 % (at 134 MPa, 12 T), and for magnet DP_101 is around 17 % (at 144 MPa, 13 T). These numbers are significantly lower than our calculation, suggesting that the midplane cables may have a stress concentration near the high field edge. The effect of the C-shape mica insulation in the stress distribution on the midplane may explain the discrepancy.

A new double aperture model magnet, called DP_102 and composed of coils 109, 112, 114 and 115, is forseen to be tested in October 2017. The coils have been recollared and the shimming has been changed, in order to reduce the stress in the midplane by 15 MPa. In case this magnet has midplane quenches, the hypothesis presented in this paper will be able to be tested at a different stress level, where we expect a lower QPV (assuming the reduction of the critical current in the midplane of these coils was reversible).

V. Conclusion

We have calculated the quench propagation velocity QPV for several quenches in six 11 T dipole model magnets. In the inner and outer pole turn, the measurements match relatively well with the simulated QPV for ATS and STS propagation mechanisms, though they match ATS at higher strain levels than STS. This suggests that the propagation in the inner and outer pole turn is strand-to-strand. In the inner midplane the relatively high QPV indicates that the quench propagates predominantly from strand to strand, rather than along the quenched strands.

A specially high QPV was observed in the midplane quenches in SP_105 and DP_101. There, the QPV is consistent with a reduction of the critical current by about 25–50 %. This reduction may be caused by the high stress in this area, and aggravated by stress concentrations due to gaps in the cables' mica insulation.

REFERENCES

[1] F. Savary *et al.*, "Progress on the Development of the Nb_3Sn 11T Dipole for the High Luminosity Upgrade of LHC," *IEEE Transactions on Applied Superconductivity*, vol. 27, no. 4, p. 4003505, June 2017.

[2] G. Willering *et al.*, "Cold Powering Tests of 11-T Nb_3Sn Dipole Models for LHC Upgrades at CERN," *IEEE Transactions on Applied Superconductivity*, vol. 26, no. 4, p. 4005604, June 2016.

[3] G. P. Willering *et al.*, "Cold Powering Performance of the First 2 m Nb_3Sn DS11T Twin-Aperture Model Magnet at CERN," *IEEE Transactions on Applied Superconductivity*, vol. 27, no. 4, p. 4002505, June 2017.

[4] G. Willering *et al.*, "Comparison of Cold Powering Performance of 2-m long Nb_3Sn 11T Model Magnets," *IEEE Transactions on Applied Superconductivity*, vol. PP, no. 99, pp. 1–1, 2018.

[5] C. Löffler *et al.*, "Finite Element Analysis of the mechanical conditions of the Nb_3Sn cable of the DS11T dipole magnet during operation," *IEEE Transactions on Applied Superconductivity*, submitted for publication in EUCAS 2017 conference; https://indico.cern.ch/event/659554/contributions/2721016/.

[6] M. Breschi *et al.*, "Quench propagation and stability analysis of rutherford resistive core cables," *Cryogenics*, vol. 46, no. 7, pp. 606 – 614, 2006, this issue contains papers from CHATS-2005: Workshop on Computation of Thermohydraulic Transients in Superconductors. [Online]. Available: http://www.sciencedirect.com/science/article/pii/S0011227506000075

[7] S. I. Bermudez *et al.*, "Quench modeling in high-field nb3sn accelerator magnets," *Physics Procedia*, vol. 67, pp. 840 – 846, 2015, proceedings of the 25th International Cryogenic Engineering Conference and International Cryogenic Materials Conference 2014. [Online]. Available: http://www.sciencedirect.com/science/article/pii/S1875389215005222

[8] G. Manfreda and Others, "Analysis of the quench propagation along nb3sn rutherford cables with the thelma code. part ii: Model predictions and comparison with experimental results," *Cryogenics*, vol. 80, pp. 364 – 373, 2016, chats on Applied Superconductivity 2015 University of Bologna, Italy, 14-16 September 2015. [Online]. Available: http://www.sciencedirect.com/science/article/pii/S001122751630073X

[9] J. L. Gomez *et al.*, "Quench Propagation Velocity and Hot Spot Temperature Models in Nb_3Sn Racetrack Coils," *IEEE Transactions on Applied Superconductivity*, vol. 28, no. 3, pp. 1–6, April 2018.

[10] L. Bottura and B. Bordini, "$J_C(B, T, \epsilon)$ Parameterization for the ITER Nb_3Sn Production," *IEEE Transactions on Applied Superconductivity*, vol. 19, no. 3, pp. 1521–1524, June 2009.

[11] J. Duvauchelle *et al.*, "Critical Current Measurements Under Transverse Pressure of a Nb_3Sn Rutherford Cable Based on 1 mm RRP Wires," *IEEE Transactions on Applied Superconductivity*, vol. PP, no. 99, pp. 1–1, 2018.